Surface & Coatings Technology 447 (2022) 128870

Contents lists available at ScienceDirect

Surface & Coatings Technology

journal homepage: www.elsevier.com/locate/surfcoat

Full length article

In situ work function measurements of W, WO_3 nanostructured surfaces

L. Marot [a,*], J. Fleury [a,b], D. Haas [a], S. Iyyakkunnel [a,c], F. Sanchez [a], R. Steiner [a], D. Mathys [d], R. Antunes [a], E. Meyer [a]

[a] Department of Physics, University of Basel, Klingelbergstrasse 82, 4056 Basel, Switzerland
[b] Solar Energy and Building Physics Laboratory, (LESO-PB), École Polytechnique Fédérale de Lausanne (EPFL), Station 18, 1015 Lausanne, Switzerland
[c] Division of Radiological Physics, Department of Radiology, University Hospital Basel, Basel, Switzerland
[d] Swiss Nanoscience Institute, University of Basel, Klingelbergstrasse 50/70, CH-4056 Basel, Switzerland

ARTICLE INFO

Keywords:
W and WO_3 nanostructured surfaces
In situ work function
Helium plasma bombardment

ABSTRACT

Surface nanostructuring enables the fabrication of materials with highly desirable properties. Nanostructured tungsten surfaces have potential applications in solar water splitting. Exposing a polished tungsten surface to helium plasma induces various surface morphological changes. Depending on the helium ion energy, temperature, and fluence, helium clusters, helium bubbles and foam-like nanostructures develop on the tungsten surface. In this study, tungsten foam-like nanostructures were formed and/or oxidised, and then examined using X-ray and ultraviolet photoelectron spectroscopy (XPS and UPS) without breaking the vacuum. The chemical state of nanostructured W or WO_3 was not modified in comparison to the pristine one. However, measuring the line width of the emitted electrons from the onset of the secondary electrons up to the Fermi edge and subtracting value from the incident photon energy, the work function acquired in situ by UPS for a nanostructured W surface increased by 0.9 eV in comparison to the pristine one. Helium ions effectively eliminated field emission sites via sputtering/implantation and thereby increased the work function. No change in work function was measured for WO_3-pristine and its fuzz: the oxidation hindered the effect of helium. In contrast to the W-fuzz sample, no helium bubbles were identified in WO_3-fuzz, as helium diffused out during oxidation.

1. Introduction

Surface nanostructuring has attracted great interest in the last few decades owing to its exceptional material properties [1]. These newly obtained mechanical, optical, and electronic properties mainly stem from the nanometer-sized micro-structures (such as grains and filaments) and the enhanced number of interfaces. The resultant higher surface area to volume ratio is especially desirable in fields like energy conversion and storage, catalysis and sensing. For instance, nanostructured materials achieve higher electrode reaction rates in lithium-ion batteries and have a higher efficiency in the photoelectrochemical splitting of water. It was reported that tungsten surfaces could be nanostructured by low-energy helium ions and after oxidation was suitable for solar water splitting applications [2], photoelectrochemical activity [3] and hydrogen gas sensing [4]. Recently, WO_3 nanostructure demonstrated photoelectrochemical performance compared to the sample without nanostructures [5].

Determining the work function (W_F) provides fundamental insight into the electronic properties of the surface of a material [6–8]. The W_F depends on the crystal structure as well as on the surface contamination and surface roughness [6,8]. Understanding the electronic states of the materials is therefore, crucial to control the electronic properties. The W_F affects the secondary ion emission [9], the field and secondary-electron emission [10,11], thermionic electron emission and thermal field emission [12]. The so-called "fuzz" tungsten, that is, tungsten with a tendril formation, was first reported by Takamura et al. [13] Low-energy helium ion bombardment of W at high temperature nanostructured the surface at high fluence. This structure is assumed to be a consequence of the formation and growth of helium bubbles that can exhibit the highest surface area to volume ratio. For the first time in 2014, Petty et al. [14,15] reported the formation of W-fuzz using the unbalanced magnetron (UBM) technique.

In this work, using a dedicated transferable sample holder, nanostructured tungsten surface was achieved using helium ion irradiation. Without breaking the vacuum, X-ray photoelectron spectroscopy (XPS) and ultraviolet photoelectron spectroscopy (UPS) were used to measure

* Corresponding author.
E-mail address: laurent.marot@unibas.ch (L. Marot).

https://doi.org/10.1016/j.surfcoat.2022.128870
Received 2 February 2022; Received in revised form 29 August 2022; Accepted 1 September 2022
Available online 9 September 2022

the surface chemical composition and W_F of the samples. Core level W4f spectra were used to determine the electronic state of the tungsten surfaces. The W_F of nanostructured W was measured for the first time via ex situ Kelvin probe using gold as reference material [16] and later using XPS [17]. However, as the Kelvin probe measurements were performed in air, the adsorbed species and the oxide on the surface hindered the results. Similarly, XPS results of Kajita et al. showed carbon and oxygen on polished and W-fuzz. The fuzz W_F was measured with O, C, and an oxidised surface. Even though the polished surface was sputtered to remove the adsorbed species and the oxide, they were not able to achieve a pure metal surface as 25 % of oxide was measured. To the best of our knowledge, we report the first in situ W_F measurement of W and WO_3 nanostructured surfaces using UPS.

2. Experimental section

The sample was prepared in a high-vacuum chamber with a background pressure under 5×10^{-6} Pa. The transferable sample holder consists of a plate where the sample is mounted between two molybdenum clamps (Fig. 1a). The molybdenum clamps act as connectors for the current and are electrically isolated from the plate using one ceramic ring and also allow for electrical biasing of the sample. Depending on the size of the sample, current up to 100 A is allowed to flow through the stripe. A bayonet locking ring was used to transfer the sample under vacuum. The W sample (99.95 %) in the form of a $30 \times 4 \times 0.1$ mm^3 stripe was clamped with the connectors to be heated. Up to 200 K temperature gradient was measured due to asymmetric contact of both wirings. One was electrically isolated and directly connected to the vacuum feedthrough. The other was placed in contact with the electrode body, which is water-cooled (Fig. 1b). UBM sputtering technique was used as He ion source. The basic principle is to unbalance the inner and outer poles of the magnetron to open the magnetic field lines [18]. To emphasise this effect, an additional coil around the magnetron enhances the outer magnets and leads to the plasma beam being shaped as a function of the coil current (Fig. 1). Helium gas at 8.5 Pa was used. After the helium exposure, one-hour annealing under oxygen at the same pressure and temperature was performed to oxidise the samples. The oxidised pristine sample was subjected to an identical oxidation process.

A retarding field energy analyser (RFEA) (model Semion Single Sensor, Impedans) was used to determine the ion flux and energy. The deposition rate was estimated using a quartz microbalance (QMB, Inficon XTM). The W morphology was investigated using a scanning electron microscope (SEM, Hitachi S-4800 field emission at 5 kV), and a focused ion beam system (FIB, Helios NanoLab 650) was used to determine the W-fuzz thickness. The temperature was measured and recorded using a pyrometer (IGAR 12-Lo, Impac at a wavelength of 1.28 μm) whose optical emissivity of bulk material was $\varepsilon = 0.38$ an. XPS measurements were performed under ultrahigh vacuum (UHV) conditions with a VG ESCALAB 210 spectrometer and monochromatic Al Kα radiation (1486.6 eV) having an energy resolution better than 0.5 eV for 20 eV pass energy. A helium discharge lamp emitting in the ultraviolet range (HeI, 21.2 eV) was used for the UPS measurements. The samples were transferred to the photoemission chamber without breaking the high-vacuum conditions. The base pressure in this chamber was around 10^{-7} Pa during acquisition. A normal electron escape angle (i.e., polar angle = 0°) and a step size of 0.025 eV were used. The Au 4f7/2 line was measured at a binding energy (BE) of 83.71 eV; hence all our XPS peaks are shifted by −0.29 eV. Wide-scan XPS spectra from 0 to 1200 eV showed only W and oxygen.

3. Results and discussion

3.1. Formation of tungsten nanostructures at different temperatures

Using the UBM, the helium ion flux was increased by increasing the magnetron power. The bias applied on the sample and the coil current was measured with the RFEA. For few parameters presented in Table 1 (Supplementary Information), the W-fuzz thickness measured by FIB is plotted against the fluence (Fig. SI 1, Supplementary Information). A similar growth rate was observed for both UBM sputtering experiments. The growth rate follows the $\sqrt{fluence}$ behaviour that was proposed by Baldwin et al. [19] and confirmed in references [15,20].

The nanostructures formed at different temperatures on a single W stripe are shown in Fig. 2 (left) for an ion energy of 60 eV and a fluence of 3.7×10^{24} m^{-2}. Owing to the temperature gradient, several topographies of He exposed surfaces evidencing pinholes and W-fuzz (Fig. 2) were imaged in one batch. The formation of W-fuzz appears in the window of temperature and He ions energies, typically assumed to be approximately 900–2000 K and 20–250 eV, respectively [21]. At 950 K, a pinhole structure similar to that reported by Petty et al. [15] in the range 1000–1100 K is shown in Fig. 2. Typically, above 1200 K, annealing hindered the formation of nanostructures. The different temperature ranges have been presented diagrammatically in Fig. 11 of reference [15].

3.2. In situ XPS and UPS of W and WO_3 nanostructures

Fig. 3 shows a comparison of the W4f and O1s core level spectra of W-fuzz and WO_3-fuzz with those of a W-pristine sample prepared by magnetron sputtering [22]. The W4f and O1s core level spectra of W-

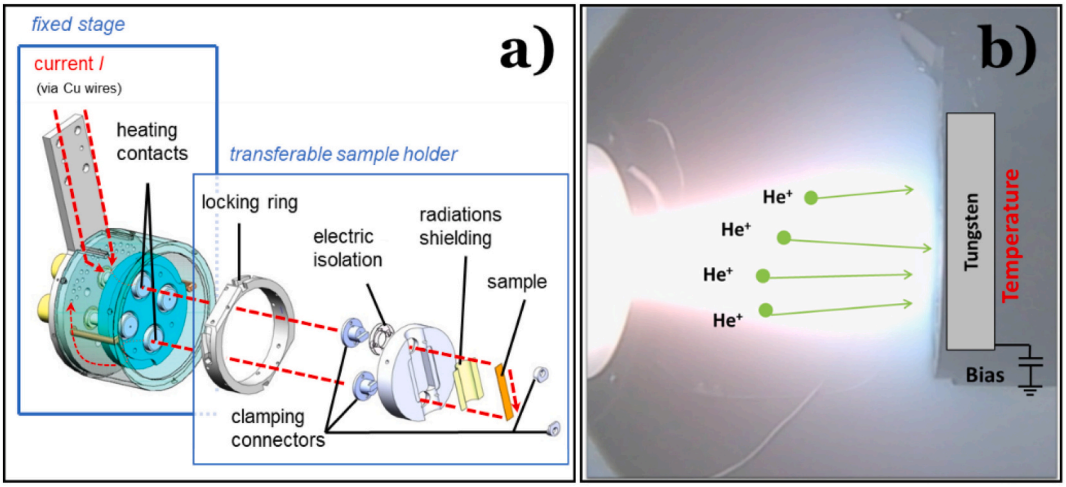

Fig. 1. a) In situ transferable sample holder for high temperature; b) helium ion beam produced by UBM sputtering.

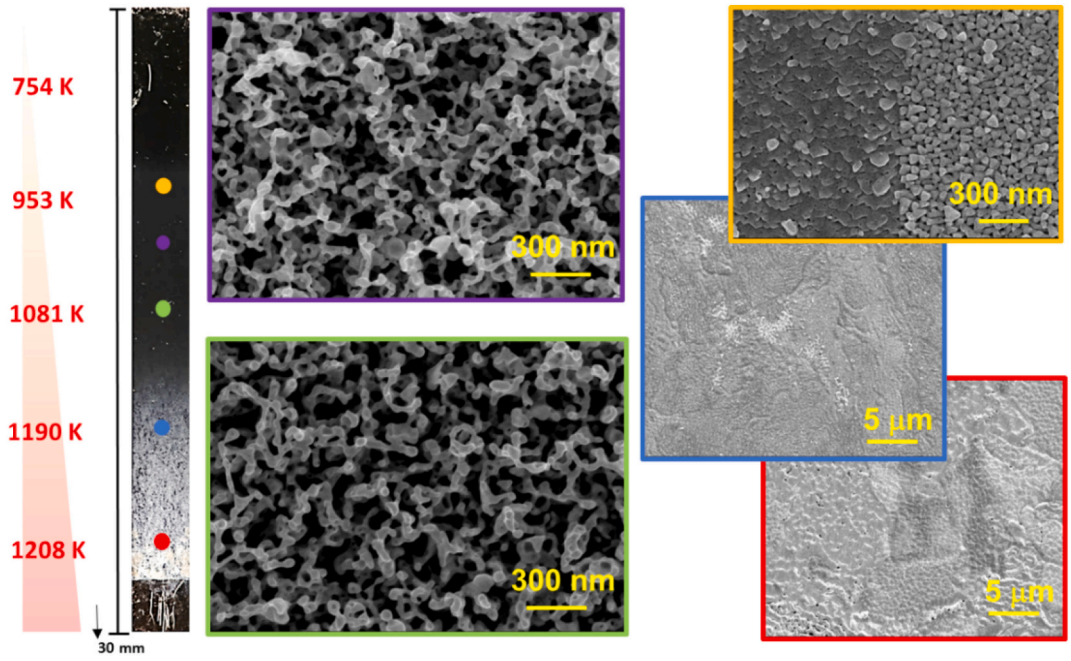

Fig. 2. W sample exposed to He ions having an energy of 60 eV and a fluence of 3.7×10^{24} m^{-2} at different temperatures with the corresponding SEM images.

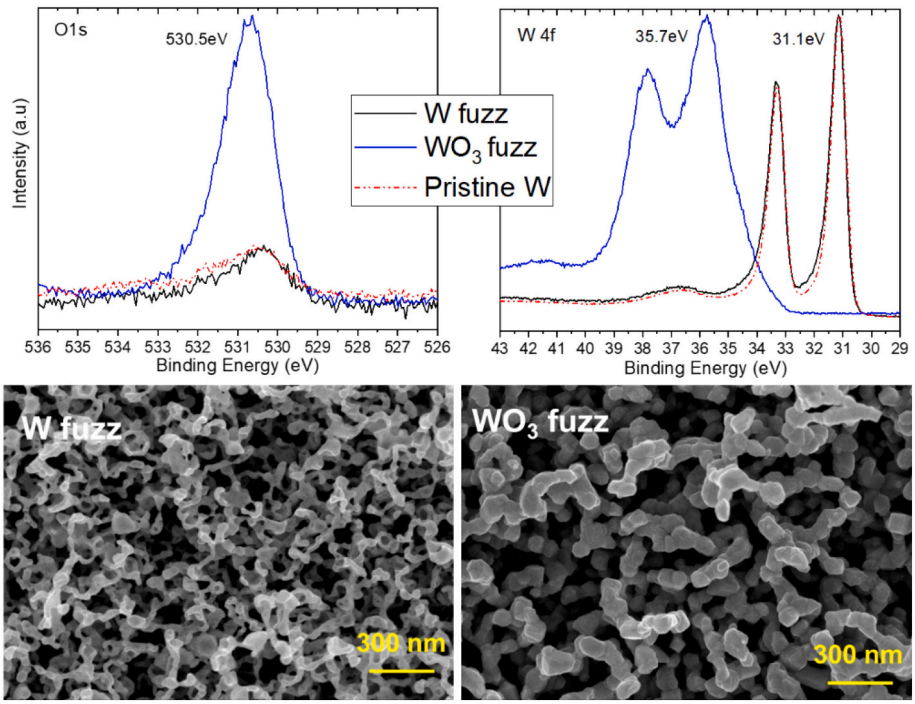

Fig. 3. W4f and O1s core level spectra of nanostructured W-fuzz and WO_3-fuzz compared with W-pristine. SEM images of W-fuzz and WO_3-fuzz obtained after exposing W surface to He ions. It corresponds to the green area of Figs. SI 2 and SI 3. (For interpretation of the references to colour in this figure legend, the reader is referred to the web version of this article.)

fuzz and W-pristine are relatively similar, with a $W4f_{7/2}$ BE of 31.1 eV. Both spectra exhibit a metallic state with oxygen adsorbed on the surface. For WO_3 nanostructures, the core level displays an oxidised state, W^{6+}, at a BE of 35.7 eV [23]. The fitting and deconvolution of the XPS spectrum revealed 15 at.% of oxidation state W^{5+} (Fig. SI 4). The morphology of the resulting WO_3-fuzz shows larger tendrils in comparison with W-fuzz as presented in the SEM images of Fig. 3. Since the temperature of the stripes was not constant for these two samples, several structures were formed. The other top-view SEM images with the corresponding XPS and UPS measurements are presented in Figs. SI 2 and SI 3. When the surface temperature was lower than 1000 K, a rough structure appeared on the surface. Nevertheless, neither pinhole nor fibre-form structures were observed. Only grooves were identified, albeit dependent on the grain orientation. Above 1150 K, fibre-form structure disappeared and a rough micrometre-sized structure with many pinholes was formed. However, for metallic or oxidised stripes, no noticeable differences were observed in the XPS and UPS measurements.

The W_F is the minimum energy needed to remove an electron from

the surface of a condensed solid to a point in the vacuum. It is given by $W_F = -e\varphi - E_F$, where e is the charge of an electron, φ is the electrostatic potential in the vacuum, and E_F is the Fermi level [5]. In this study, photoemission by means of in situ UPS was used to measure W_F. If the energy of the incoming photon is greater than the substrate's W_F, photoelectric emission occurs. The measured value is highly sensitive to the surface cleanliness and homogeneity for a single metal. Changes in W_F are often observed over time due to contamination from within the UHV chamber [5]. The minimum energy required to emit an electron from the surface into the vacuum is the photon energy of the metal minus the secondary-electron cut-off energy of the UPS spectrum: $W_F = h\upsilon - E_{cutoff}$, where $h\upsilon$ is the energy of the incoming photons (21.2 eV) emitted by the He discharge lamp.

Fig. 4 shows the UPS spectra of W-pristine, W-fuzz and WO_3-fuzz. In Fig. 4b, it can be seen that both W-pristine and W-fuzz exhibit one main peak at 2.3 eV, which corresponds to the W5d orbital. The second one, around 5.6 eV, is attributed to the O2p orbitals. The last peak at 12.1 eV (Fig. 4b) appears only for polished W and arises from the W5d–O2p orbital mixing. A significant difference in the UPS line shape between W and WO_3 is the shift observed in the oxide spectrum near the E_F (Fig. 4c). WO_3 is a semiconductor and thus features a band gap between the valence and conduction bands. The two small peaks at 0.80 and 2.34 eV correspond to the under-stoichiometric W oxide, which comes from the 15 at.% W^{5+} identified on the W4f core level data (Fig. SI 4). The peak at 0.8 eV means that a new occupied state is formed inside the band gap, while the peak at 2.84 eV represents the valence-band maximum, i.e., the lowest band gap limit of a semiconductor. The peak at approximately 4.4 eV on the WO_3 spectrum is assigned to an O2p-derived band and the shoulder around 6 eV is assigned to a hybridised W5d–O2p band [24–26]. Fig. 4a shows the evolution of the high BE cut-off of the UPS spectra: W_F decreases from 6.1 eV for WO_3-fuzz to 5.77 eV for W-fuzz and to 4.78 eV for W-pristine. The resulting W_F can be derived by a linear extrapolation at the edge where the intensity reaches zero, as shown in Fig. 4a. Several areas of the strip were characterized for W-fuzz and WO_3-fuzz (Figs. SI 2 and SI 3). The W_F was calculated for different growth rates of W-fuzz and WO_3-fuzz and are indicated in the SI.

3.3. Discussion of the W_F of W and WO_3 nanostructures

Fig. 5 shows a comparison of the W_F of W and WO_3 (polished and fuzz) determined in this work to the previously reported results.

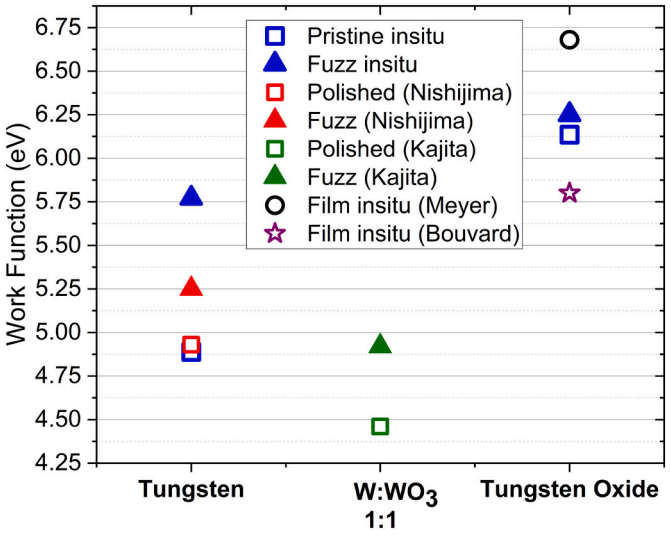

Fig. 5. Comparison of the W_F of W-fuzz and WO_3-fuzz to polished tungsten and other values from the literature: Nishijima et al. [16] measured ex situ with a Kelvin probe. Kajita et al. [17] compared polished and fuzz for a mixture of 50 % W and 50 % WO_3 measured by ex situ XPS. Meyer et al. and Bouvard et al. report in situ measurements of WO_3 [27,30].

Nishijima [15] used ex situ Kelvin probe measurements using gold as the reference material; the chemical state of the surface was not stated. Kajita et al. [16] measured the W_F of 1:1 W:WO_3 using XPS valence-band spectra. The figure also includes measurements performed without breaking the vacuum. Meyer et al. [27] evaporated WO_3 on silicon using a Knudsen effusion method; Bouvard et al. [23] used magnetron sputtering with an Ar/O_2 gas mixture. Our in situ measurements revealed a W_F of approximately 5.75 eV for W-fuzz. In contrast, the W_F of W-fuzz reported by Nishijima et al. is approximately 0.5 eV lower. However, it is worth mentioning that their value was obtained with Kelvin probe measurements in air and thus with a contaminated surface. As reported by Greiner et al., in the case of nickel oxide [28], the W_F of ex situ NiO is significantly lower than the W_F of in situ NiO due to hydroxylation of the surface. The W_F of 1:1 W:WO_3-fuzz reported by Kajita et al. is approximately 4.75 eV, and this value was obtained in-vacuo after argon sputtering. As reported by Vida et al. [29], the chemical state of the

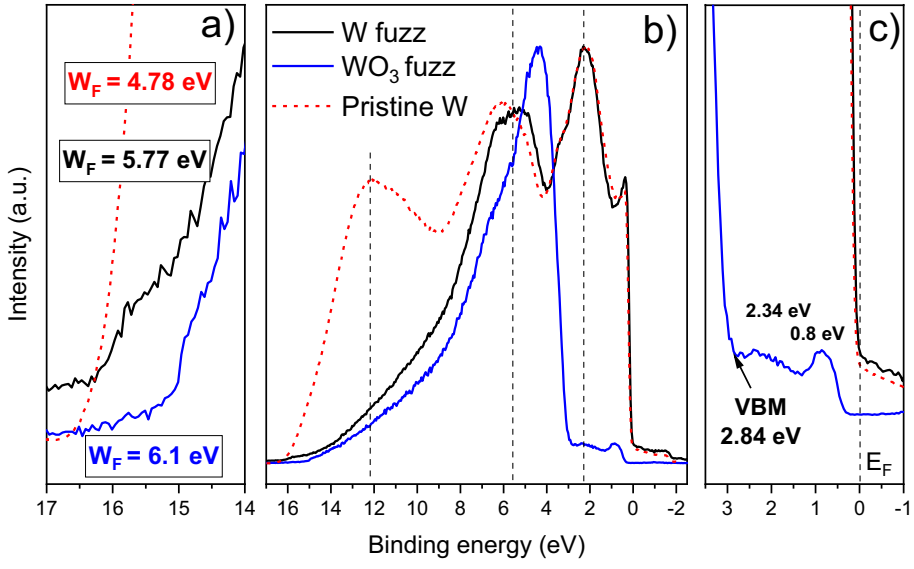

Fig. 4. He I UPS photoemission spectra of W-fuzz, WO_3-fuzz and W-pristine: (a) secondary-electron cut-off region, (b) expanded view of the valence band spectra and (c) near E_F region.

surface influences the W_F and the W_F measured by Kajita et al. was between the W_F of metallic W and WO_3.

In our study, the W_F of W-fuzz is approximately 0.8 eV greater than that of the W-pristine. This result could be counter-intuitive since, as previously reported [31,32], the W_F of metals tends to decrease with an increase in surface roughness. Although Petty [15] reported a fuzz roughness determined using a confocal microscope, we consider that the fuzz structure displayed in Fig. 3 cannot be accurately represented in terms of a roughness value. The results suggest that the tendril structure and the higher surface area for W-fuzz may increase the energy needed to remove the valence electrons from the surface. Moreover, it is known that the W_F of tungsten single crystal varies from 4.47 to 5.25 eV depending on the (111), (100), and (110) plane orientations [33]. Instead, a W-pristine coated film is polycrystalline [34], and therefore, an average contribution from all crystalline orientations to W_F is determined with UPS. Since Ohno et al. [35] have demonstrated that W-fuzz has a random orientation, the W_F reported in this study is also an average contribution from all crystalline orientations. According to Grubbs et al. [36], the higher W_F of a metal oxide when compared to that of the pure metal cannot be attributed to a change in the crystalline structure, presence of strain, or any residual oxygen in the bulk. Instead, it is thought to be caused by the incorporation of oxygen from the growth environment into the W layer and therefore the oxygen-rich layer reduces the chemical gradient that would tend to pull the oxygen out of the oxide. The W_F is observed to increase by approximately 1.3 eV from W-pristine to WO_3-pristine and by 0.6 eV from a W-fuzz to a WO_3-fuzz. Although no W_F values for a fully WO_3-fuzz surface were found in the literature, a similar behaviour was reported by Kajita [37] for polished and nanostructured 1:1 W:WO_3 samples. They found that the W_F of the fuzz sample increased by 0.5 eV.

When compared to a WO_3-pristine sample, an increase of approximately 0.12 eV in W_F of WO_3-fuzz can be observed (Fig. 5). This increase is significantly smaller than the 0.9 eV obtained in the metal case. In comparison, Bouvard reported for pristine surface a W_F value of 5.8 eV for WO_3 and 6.0 eV for $WO_{2.7}$ [30]. It is close to our value (6.13 eV), considering that our W-pristine and WO_3-fuzz have a component of oxidation state 5+ (Fig. SI 4). As reported by BastaniNejad et al., measurements and accompanying simulation results obtained using Stopping and Range of Ions in Matter (SRIM) [38] suggest that ion resulting in gas conditioning effectively eliminates field emission sites via sputtering and ion implantation, thereby increasing the W_F of the electrodes [39]. The simulation results also support the general trend that helium gas conditioning is more effective at lower voltages because it yields a shallow implantation depth, which is better suited to increase the W_F of the metal. These results were obtained at energies similar to those used in our work, i.e., 60 eV. Moreover, transmission electron microscopy images revealed that W-fuzz stored helium bubbles in the dendrites [40]. Therefore, since the W_F of WO_3-pristine and WO_3-fuzz are similar, one explanation might be that the oxygen in the W lattice and the removal of He from the surface and subsurface by oxygen during the one-hour long oxidation hinders the He effect. Fig. 6a, b, d, and e presents cross-section SEM images of the WO_3-fuzz sample using FIB (the corresponding top-view SEM image of the sample is presented in Fig. 3). The WO_3 filament structure does not exhibit typical He bubble reported in W-fuzz [40–42]. Voids in between the filaments were observed but no helium bubbles were seen inside the tendrils. For comparison, Fig. 6c and f presents the W-fuzz cross-section (refer to Fig. 3 for top-view). Helium bubbles in the filaments of the W-fuzz structure are revealed in these images. As explained above, one of the main effects concerning the W_F increase is the helium implantation, which is also demonstrated by the higher W_F obtained in other structures on the W stripe exposed for the same He fluence but at different temperatures (Fig. SI 2). Also, the W_F determined for pinhole-W and nano-W structures show a variation of $<$0.5 eV (Fig. SI 2). For a high coverage of He on a metal surface, a large increase in the W_F was measured by Kolesnychenko et al. [43]. This corroborates the fact that an increase in the surface roughness does not necessarily translate into a decrease in W_F. Moreover, Kajita et al. [17] reported an increase in the Ra value from 0.1 to 1 μm and an increase in the W_F from pristine to fuzz surfaces.

4. Conclusion

In situ core level and valence-band photoelectron spectroscopy were used to investigate the effect of the surface morphology of tungsten and tungsten oxide on their W_F. It was shown that the surface topography and the oxidation of tungsten strongly influence the W_F of the material. An increase of 0.9 eV in the W_F was observed from W-pristine to W-fuzz. These observations can be explained by the low-energy He bombardment, which effectively eliminates field emission sites via sputtering and ion implantation, thereby increasing the W_F of the electrode. In comparison to Nishijima, the W_F reported for air-contaminated W-fuzz is 0.5 eV lower than our value; this highlight the need for in situ measurement. Moreover, for the first time, WO_3-fuzz's W_F was measured and also shows an increase from tungsten to tungsten oxide. No significant

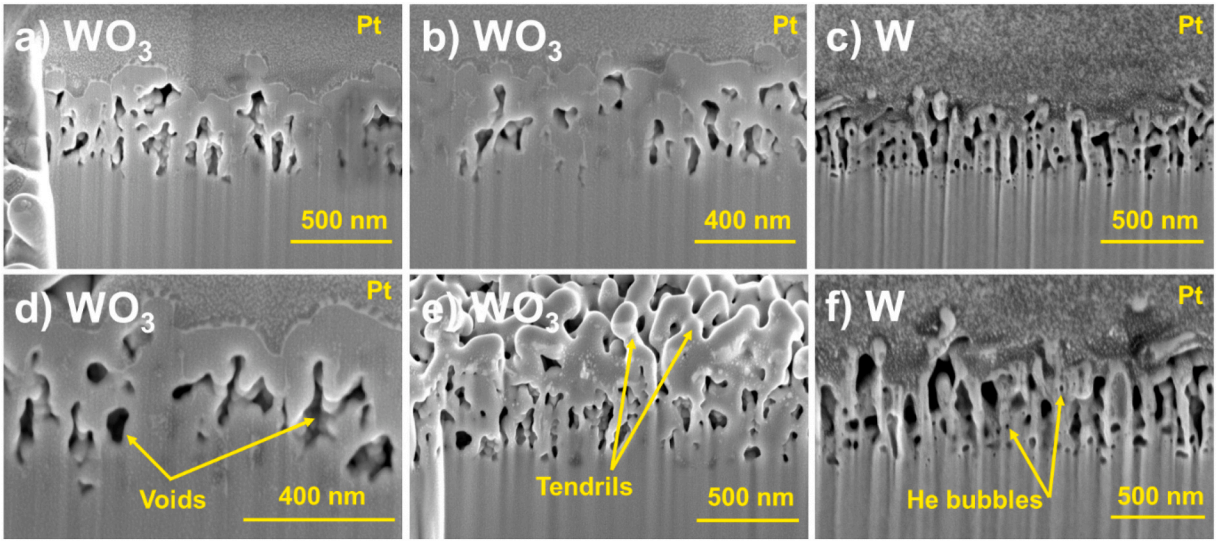

Fig. 6. FIB cross-section SEM images of the W-fuzz and WO_3-fuzz sample. Image (e) was obtained without a platinum protection layer. Top-view SEM images of the W-fuzz and WO_3-fuzz are presented in Fig. 3.

change was measured from WO_3-pristine to WO_3-fuzz since the helium bubbles observed in the W-fuzz filament might disappear for the WO_3-fuzz during the oxidation step. In contradiction, Kajita did not evidence this effect as the W-fuzz was not fully oxidised.

Electrochemical reaction on surfaces is related to the work function of material and the high W and WO_3 nanostructures W_F might play an important role for photocatalytic reaction with visible light. For example, high work function metal oxides material, like tungsten oxide, has an excellent ability to form a hole-selective contact for a crystalline silicon solar cells absorber [44]. Having a WO_3-fuzz structure may improve the hole extraction for this application. Moreover, in the case of surface arcing, the field emission can be linked to the surface W_F. Unipolar arcing is a crucial issue for metallic fusion reactors, and this study will bring more insight into the case of nanostructured W surfaces. Comparison of W_F measurements using UPS and Kelvin probe under vacuum is foreseen to develop this work further.

Funding sources

The authors would like to thank the Swiss Federal Office of Energy, Swiss Nanoscience Institute, Swiss National Science Foundation and the Federal Office for Education and Science for their financial support.

CRediT authorship contribution statement

The manuscript was written through contributions of all authors. All authors have given approval to the final version of the manuscript. R.S. designed the electrode used in this work, S.I. mounted it. J.F., D.H. and F.S. performed the experiments. The SEM and FIB images were done by D.M. L.M. performed data analysis, validation and review. L.M. and R.A. performed editing.

Declaration of competing interest

The authors declare that they have no known competing financial interests or personal relationships that could have appeared to influence the work reported in this paper.

Data availability

Data will be made available on request.

Appendix A. Supplementary data

The following files are available free of charge.

Table of parameters used for the UBM process

W-fuzz thickness as a function of the fluence

Tungsten sample exposed to He ions at different temperature with the corresponding SEM images and the XPS and UPS measurements

Oxidised tungsten sample exposed to He ions at different temperature with the corresponding SEM images and the XPS and UPS measurements

Supplementary data to this article can be found online at https://doi.org/10.1016/j.surfcoat.2022.128870.

References

[1] İ. Tanyeli, L. Marot, M.C.M. van de Sanden, G. De Temmerman, Nanostructuring of iron surfaces by low-energy helium ions, ACS Appl. Mater. Interfaces 6 (5) (2014) 3462–3468, https://doi.org/10.1021/am405624v.

[2] M. de Respinis, G. De Temmerman, I. Tanyeli, M.C.M. van de Sanden, R.P. Doerner, M.J. Baldwin, R. van de Krol, Efficient plasma route to nanostructure materials: case study on the use of m-WO3 for solar water splitting, ACS Appl. Mater. Interfaces 5 (15) (2013) 7621–7625, https://doi.org/10.1021/am401936q.

[3] H. Fan, Z. Wu, T. Sun, M. Yang, J. Guo, K. Yang, Y. Li, Efficient plasma-assisted approach in nanostructure fabrication of tungsten, Mater. Des. 89 (2016) 78–84, https://doi.org/10.1016/j.matdes.2015.09.139.

[4] Y. Kimura, K. Ibano, K. Uehata, I. Hirai, H. Tae Lee, Y. Ueda, Improved hydrogen gas sensing performance of WO3 films with fibrous nanostructured surface, Appl. Surf. Sci. 532 (2020), 147274, https://doi.org/10.1016/j.apsusc.2020.147274.

[5] S. Feng, S. Kajita, M. Higashi, A. Bieberle-Hütter, T. Yoshida, N. Ohno, Photoelectrochemical properties of plasma-induced nanostructured tungsten oxide, Appl. Surf. Sci. 580 (2022), 151979, https://doi.org/10.1016/j.apsusc.2021.151979.

[6] J.W. Kim, A. Kim, Absolute work function measurement by using photoelectron spectroscopy, Curr. Appl. Phys. 31 (2021) 52–59, https://doi.org/10.1016/j.cap.2021.07.018.

[7] C. Ko, Z. Yang, S. Ramanathan, Work function of vanadium dioxide thin films across the metal-insulator transition and the role of surface nonstoichiometry, ACS Appl. Mater. Interfaces 3 (9) (2011) 3396–3401, https://doi.org/10.1021/am2006299.

[8] M. Yoshitake, Work Function and Band Alignment of Electrode Materials: The Art of Interface Potential for Electronic Devices, Solar Cells, and Batteries, Springer Nature, 2020.

[9] M.L. Yu, Matrix effects in the work-function dependence of negative-secondary-ion emission, Phys. Rev. B 26 (8) (1982) 4731–4734, https://doi.org/10.1103/PhysRevB.26.4731.

[10] C.E. Huerta, M.I. Patino, R.E. Wirz, Secondary electron emission from textured surfaces, J. Phys. Appl. Phys. 51 (14) (2018), 145202, https://doi.org/10.1088/1361-6463/aab1ac.

[11] M. Patino, Y. Raitses, R. Wirz, Secondary electron emission from plasma-generated nanostructured tungsten fuzz, Appl. Phys. Lett. 109 (20) (2016), 201602, https://doi.org/10.1063/1.4967830.

[12] D. Sinelnikov, D. Bulgadaryan, V. Kurnaev, M. Lobov, The model of thermal field emission from tungsten fuzz, J. Phys. Conf. Ser. 941 (2017), 012024, https://doi.org/10.1088/1742-6596/941/1/012024.

[13] S. Takamura, N. Ohno, D. Nishijima, S. Kajita, Formation of nanostructured tungsten with arborescent shape due to helium plasma irradiation, Plasma Fusion Res. 1 (2006), https://doi.org/10.1585/pfr.1.051, 051-051.

[14] T.J. Petty, J.W. Bradley, Tungsten nanostructure formation in a magnetron sputtering device, J. Nucl. Mater. 453 (1–3) (2014) 320–322, https://doi.org/10.1016/j.jnucmat.2014.07.023.

[15] T.J. Petty, A. Khan, T. Heil, J.W. Bradley, Fuzzy tungsten in a magnetron sputtering device, J. Nucl. Mater. 480 (2016) 374–385, https://doi.org/10.1016/j.jnucmat.2016.08.019.

[16] D. Nishijima, R.P. Doerner, Work function studies of plasma-exposed tungsten surfaces, in: 14th PFMC Conference, 2013.

[17] S. Kajita, A. Ohta, T. Ishida, K. Makihara, T. Yoshida, N. Ohno, Increase in the work function of W/WO 3 by helium plasma irradiation, Jpn. J. Appl. Phys. 54 (12) (2015), 126201, https://doi.org/10.7567/JJAP.54.126201.

[18] B. Window, N. Savvides, Unbalanced dc magnetrons as sources of high ion fluxes, J. Vac. Sci. Technol. A 4 (3) (1986) 453–456, https://doi.org/10.1116/1.573904.

[19] M.J. Baldwin, R.P. Doerner, Helium induced nanoscopic morphology on tungsten under fusion relevant plasma conditions, Nucl. Fusion 48 (3) (2008), 035001, https://doi.org/10.1088/0029-5515/48/3/035001.

[20] T.J. Petty, M.J. Baldwin, M.I. Hasan, R.P. Doerner, J.W. Bradley, Tungsten 'Fuzz' growth re-examined: the dependence on ion fluence in non-erosive and erosive helium plasma, Nucl. Fusion 55 (9) (2015), 093033, https://doi.org/10.1088/0029-5515/55/9/093033.

[21] K.D. Hammond, Helium, hydrogen, and fuzz in plasma-facing materials, Mater. Res. Express 4 (10) (2017), 104002, https://doi.org/10.1088/2053-1591/aa8c22.

[22] S. Iyyakkunnel, L. Marot, B. Eren, R. Steiner, L. Moser, D. Mathys, M. Düggelin, P. Chapon, E. Meyer, Morphological changes of tungsten surfaces by low-flux helium plasma treatment and helium incorporation via magnetron sputtering, ACS Appl. Mater. Interfaces 6 (14) (2014) 11609–11616, https://doi.org/10.1021/am502370t.

[23] O. Bouvard, A. Krammer, A. Schüler, In situ Core-level and valence-band photoelectron spectroscopy of reactively sputtered tungsten oxide films, Surf. Interface Anal. 48 (7) (2016) 660–663, https://doi.org/10.1002/sia.5927.

[24] Y. Du, K.H.L. Zhang, T. Varga, S.A. Chambers, Reflection high-energy electron diffraction beam-induced structural and property changes on WO3 thin films, Appl. Phys. Lett. 105 (5) (2014), 051606, https://doi.org/10.1063/1.4892810.

[25] M. Vasilopoulou, A. Soultati, D.G. Georgiadou, T. Stergiopoulos, L.C. Palilis, S. Kennou, N.A. Stathopoulos, D. Davazoglou, P. Argitis, Hydrogenated under-stoichiometric tungsten oxide anode interlayers for efficient and stable organic photovoltaics, J. Mater. Chem. A 2 (6) (2014) 1738–1749, https://doi.org/10.1039/C3TA13975A.

[26] F.Y. Xie, L. Gong, X. Liu, Y.T. Tao, W.H. Zhang, S.H. Chen, H. Meng, J. Chen, XPS studies on surface reduction of tungsten oxide nanowire film by Ar+ bombardment, J. Electron Spectrosc. Relat. Phenom. 185 (3) (2012) 112–118, https://doi.org/10.1016/j.elspec.2012.01.004.

[27] J. Meyer, M. Kröger, S. Hamwi, F. Gnam, T. Riedl, W. Kowalsky, A. Kahn, Charge generation layers comprising transition metal-oxide/organic interfaces: electronic structure and charge generation mechanism, Appl. Phys. Lett. 96 (19) (2010), 193302, https://doi.org/10.1063/1.3427430.

[28] M.T. Greiner, M.G. Helander, Z.-B. Wang, W.-M. Tang, Z.-H. Lu, Effects of processing conditions on the work function and energy-level alignment of NiO thin films, J. Phys. Chem. C 114 (46) (2010) 19777–19781, https://doi.org/10.1021/jp108281m.

[29] G. Vida, V.K. Josepovits, M. Győr, P. Deák, Characterization of tungsten surfaces by simultaneous work function and secondary electron emission measurements, Microsc. Microanal. 9 (4) (2003) 337–342, https://doi.org/10.1017/S143192760303023X.

[30] O.V.C. Bouvard, Coatings with Tailored Electronic and Optical Properties for Advanced Glazing, EPFL, Lausanne, 2019, https://doi.org/10.5075/epfl-thesis-9199.
[31] W. Li, D.Y. Li, On the correlation between surface roughness and work function in copper, J. Chem. Phys. 122 (6) (2005), 064708, https://doi.org/10.1063/1.1849135.
[32] G.A. Somorjai, Y. Li, Introduction to Surface Chemistry and Catalysis, John Wiley & Sons, 2010.
[33] H. Ishii, K. Sugiyama, E. Ito, K. Seki, Energy level alignment and interfacial electronic structures at organic/metal and organic/organic interfaces, Adv. Mater. 11 (8) (1999) 605–625, https://doi.org/10.1002/(SICI)1521-4095(199906)11:8<605::AID-ADMA605>3.0.CO;2-Q.
[34] L. Marot, R. Steiner, M. Gantenbein, D. Mathys, E. Meyer, Co-deposition of rhodium and tungsten films for the first-Mirror on ITER, J. Nucl. Mater. 415 (1) (2011) S1203–S1205, https://doi.org/10.1016/j.jnucmat.2010.08.062.
[35] N. Ohno, Y. Hirahata, M. Yamagiwa, S. Kajita, M. Takagi, N. Yoshida, R. Yoshihara, T. Tokunaga, M. Tokitani, Influence of crystal orientation on damages of tungsten exposed to helium plasma, J. Nucl. Mater. 438 (2013) S879–S882, https://doi.org/10.1016/j.jnucmat.2013.01.190.
[36] M.E. Grubbs, M. Deal, Y. Nishi, B.M. Clemens, The effect of oxygen on the work function of tungsten gate electrodes in MOS devices, IEEE Electron Device Lett. 30 (9) (2009) 925–927, https://doi.org/10.1109/LED.2009.2026717.
[37] S. Kajita, T. Yoshida, D. Kitaoka, R. Etoh, M. Yajima, N. Ohno, H. Yoshida, N. Yoshida, Y. Terao, Helium plasma implantation on metals: nanostructure formation and visible-light photocatalytic response, J. Appl. Phys. 113 (13) (2013), 134301, https://doi.org/10.1063/1.4798597.
[38] J.F. Ziegler, M.D. Ziegler, J.P. Biersack, SRIM – the stopping and range of ions in matter (2010), Nucl. Instrum. Methods Phys. Res. Sect. B Beam Interact. Mater. At. 268 (11) (2010) 1818–1823, https://doi.org/10.1016/j.nimb.2010.02.091.
[39] M. BastaniNejad, A.A. Elmustafa, E. Forman, J. Clark, S. Covert, J. Grames, J. Hansknecht, C. Hernandez-Garcia, M. Poelker, R. Suleiman, Improving the performance of stainless-steel DC high voltage photoelectron gun cathode electrodes via gas conditioning with helium or krypton, Nucl. Instrum. Methods Phys. Res. Sect. Accel. Spectrometers Detect. Assoc. Equip. 762 (2014) 135–141, https://doi.org/10.1016/j.nima.2014.05.114.
[40] S. Kajita, N. Yoshida, R. Yoshihara, N. Ohno, M. Yamagiwa, TEM observation of the growth process of helium nanobubbles on tungsten: nanostructure formation mechanism, J. Nucl. Mater. 418 (1–3) (2011) 152–158, https://doi.org/10.1016/j.jnucmat.2011.06.026.
[41] E. Gao, W. Nadvornick, R. Doerner, N.M. Ghoniem, The influence of low-energy helium plasma on bubble formation in micro-engineered tungsten, J. Nucl. Mater. 501 (2018) 319–328, https://doi.org/10.1016/j.jnucmat.2018.01.040.
[42] P. McCarthy, D. Hwangbo, M. Bilton, S. Kajita, J.W. Bradley, Enhanced fuzzy tungsten growth in the presence of tungsten deposition, Nucl. Fusion 60 (2) (2020), 026012, https://doi.org/10.1088/1741-4326/ab6060.
[43] O.Yu. Kolesnychenko, O.I. Shklyarevskii, H. van Kempen, Anomalous increase of the work function in metals due to adsorbed helium, Phys. B Condens. Matter 284–288 (2000) 1257–1258, https://doi.org/10.1016/S0921-4526(99)02519-3.
[44] M. Bivour, J. Temmler, H. Steinkemper, M. Hermle, Molybdenum and tungsten oxide: high work function wide band gap contact materials for hole selective contacts of silicon solar cells, Sol. Energy Mater. Sol. Cells 142 (2015) 34–41, https://doi.org/10.1016/j.solmat.2015.05.031.